J Mater Sci (2012) 47:508–513
DOI 10.1007/s10853-011-5827-7

Size control and magnetic properties of single layer monodisperse Ni nanoparticles prepared by magnetron sputtering

Tangchao Peng · Xiangheng Xiao · Wei Wu · Lixia Fan · Xiaodong Zhou · Feng Ren · Changzhong Jiang

Received: 24 February 2011 / Accepted: 26 July 2011 / Published online: 4 August 2011

Abstract Single layer monodisperse Ni nanoparticles were successfully prepared by reductive annealing of NiO films formed by magnetron sputtering. The spherical Ni nanoparticles had a monodisperse distribution on the substrate. The formation process of Ni nanoparticles was investigated, and the Ni nanoparticle size can be precisely controlled by the magnetron sputtering time. Morphology of these nanoparticles was observed with scanning electron microscopes and transmission electron microscopes. Magnetic properties of Ni nanoparticles have been confirmed by using a vibration sample magnetometer. The blocking temperature, particle size, and effective anisotropy constant were calculated by fitting the relationship between coercivity and temperature.

T. Peng · X. Xiao · W. Wu · X. Zhou · F. Ren · C. Jiang
Key Laboratory of Artificial Micro- and Nano-structures of Ministry of Education, Wuhan University, Wuhan 430072, People's Republic of China

T. Peng · X. Xiao (✉) · W. Wu · X. Zhou · F. Ren · C. Jiang (✉)
Center for Electron Microscopy and School of Physics and Technology, Wuhan University, Wuhan 430072, People's Republic of China
e-mail: xxh@whu.edu.cn

C. Jiang
e-mail: czjiang@whu.edu.cn

X. Xiao
State Key Laboratory of Electronic Thin Films and Integrated Devices, University of Electronic Science and Technology of China, Chengdu 610054, People's Republic of China

L. Fan
School of Materials and Metallurgy, Wuhan University of Science and Technology, Wuhan 430081, People's Republic of China

Introduction

Magnetic properties of nanoparticles are a rapid-growing field that involves multiple disciplines such as material science, condensed matter physics, biology, medicine, and planetary science [1–5]. Compared with bulk materials, magnetic nanoparticles show a wide variety of unusual magnetic properties which are associated with the internal magnetic order, such as superparamagnetism [6], quantum tunneling of magnetization [7], enhanced magnetic coercivity [8], and other characteristics associated with core–shell structures [9, 10]. Magnetic properties of nanoparticles are strongly influenced by so-called finite-size and surface effects. Among the ferromagnetic 3d transition elements Fe, Ni, and Co, the nanosized ferromagnetic Ni is being widely studied as it both arouses an interest in the field of fundamental sciences and presents a possibility for applications such as magnetic storage, ferrofluids, medical diagnosis, multilayer capacitors, and especially catalysis. Because these properties and their applications can be tuned by controlling the size and structure of the particles, the development of flexible and precise synthetic routes has been a hot spot of research [11]. Ni nanoparticles have been made using a variety of techniques such as thermal decomposition [12], sol–gel [13], spray pyrolysis [14], high-energy ball milling [15], chemical synthesis [16], cluster beam deposition [17], and magnetron sputtering [18]. In Ref. [16], the Ni nanoparticles were prepared by chemical synthesis, and exist as powder form or in the solution. In Ref. [17], Ni and Ni–NiO core–shell nanoclusters with cubic shape were fabricated by magnetron-plasma-based cluster beam deposition. In Ref. [18], Ni nanoparticles were deposited on Si substrate by magnetron sputtering, and formed the Ni nanoparticle films. However, it is difficult to obtain single layer monodisperse Ni

nanoparticles by means of these techniques. The single layer Ni nanoparticles can be obtained by annealing the Ni thin films [19]. But, the thickness of the Ni thin film has to be limited to several nanometers, and the uniformity of the particle size and shape is difficult to control. This article introduces an easy and novel technique to obtain single layer Ni particles with controllable size on substrate. The Ni nanoparticles are separately scattered on substrate, and their intrinsic features will be displayed.

Experiment

NiO films approximately 100, 50, 30, 20, and 10 nm in thickness were deposited from a Ni target (ca. 50 mm in diameter, thickness of 3 mm, and 99.99% pure) onto Si(111) by a DC reactive magnetron sputtering system (ULVAC, ACS-4000-C4) at room temperature, and the samples were labeled #1–5. The substrate–target distance was 150 mm. Sputtering was performed at a constant power of 120 W. A gas mixture of oxygen and argon with a ratio of 1:2 was used as the sputtering gas with a total pressure of 0.78 Pa. All of the samples were annealed at 800 °C in hydrogen gas for 1 h. The size distribution and the morphology of the Ni nanoparticles were studied through field emission scanning electron micrograph (FE-SEM) with a FEI Nova 400 Nano. Transmission electron microscopy (TEM, JEOL JEM-2010) was performed to analyze the nanoparticles which were scraped off the substrate. The structure and crystallinity of the single layer particles were investigated through grazing incidence X-ray diffraction (GIXRD) by using PANalytical B.V X'Pert PRO. A monochromatic CuKα radiation source ($\lambda = 0.15418$ nm) was used in the step scanning mode with steps of 0.02° and a scanning speed of 4°/min. The magnetic hysteresis loops of samples #1–5 were measured at room temperature with a vibration sample magnetometer (VSM) and a quantum design PPMS. Samples #4 and #5 exhibited superparamagnetism at room temperature, and the coercivity of sample #4 was further measured in the temperature range of 5–300 K. The direction of the magnetic field was along the plane of the substrate.

Results and discussion

SEM analysis is performed in the series to confirm the presence of Ni nanoparticles and determine their size distribution. The SEM images of the single layer Ni nanoparticles of samples #1–5 are shown in Fig. 1a–e, respectively. Obviously, the NiO films are reduced to the extent that the single layer Ni nanoparticles are monodisperse on the Si substrate. Typical images obtained from the SEM investigation of the samples studied, accompanied by their histograms, are displayed in Fig. 1f–j. The histograms are constructed by counting hundreds of Ni nanoparticles spread out in different zones of the SEM images and considering a normal distribution. The images obtained from SEM investigation indicate that the Ni nanoparticles are homogeneously distributed on the Si substrate, forming a nearly spherical shape. For example, the relevant size parameter of sample #1 is a median diameter $d_0 = 126.89$ nm, as estimated with the normal distribution function. In order to further confirm the structure of the particles, TEM is performed to analyze the nanoparticles which are scraped off the substrate. Bright field TEM micrograph and electron diffractogram of the nanoparticles of sample #4 are presented in Fig. 2. The particle size is consistent with the SEM results in Fig. 1d, and all of these particles are nearly spherical. The electron diffraction pattern shows typical diffraction rings which confirm face centered cubic (fcc) Ni crystal structure particles with a 0.357-nm lattice constant.

Figure 3 shows the GIXRD diffraction patterns which are recorded for samples #1–5. All of the samples show the presence of diffraction peaks from the (111) and (200) lattice planes of the Ni lattice and the (200) lattice planes of the NiO lattice. Ni (111) peak shows a slight decrease in intensity with the decreasing particle size, and the intensity of Ni (111) peak has nearly disappeared in samples #4 and #5. The NiO (200) peak shows the presence of NiO in samples #1–5. The intensity of these NiO (200) peaks is very low, and the peaks are very wide. It can be concluded that the NiO may come from the incompletely reduced NiO film or the oxide coating on the surface of the Ni particles.

The proposed formation mechanism should be a simple reduction process because of the annealing treatment in hydrogen atmosphere, the Ni nanoparticles have formed eventually as follows:

$$\mathrm{NiO} + \mathrm{H_2} \xrightarrow{\Delta} \mathrm{Ni} + \mathrm{H_2O} \uparrow$$

In order to investigate the relationship between particle size and film thickness, we assume that the NiO film is reduced to form Ni island thin films initially. Then, the Ni nanoparticles with lower Gibbs free energy will be formed by heating treatment of the Ni thin films [20]. The thermodynamic basis for the formation of Ni nanoparticles, based on nucleation, had been discussed by Jiang [21], Liang [22], and Sanjabi [23]. Jiang [21] suggested a model for prediction of the dimensional conditions for transition from a Ni thin film to Ni particles. Based on their model, and considering the size dependence of nanosolid melting points, the diameter of a transformed particle is predicted to be 3 times larger than

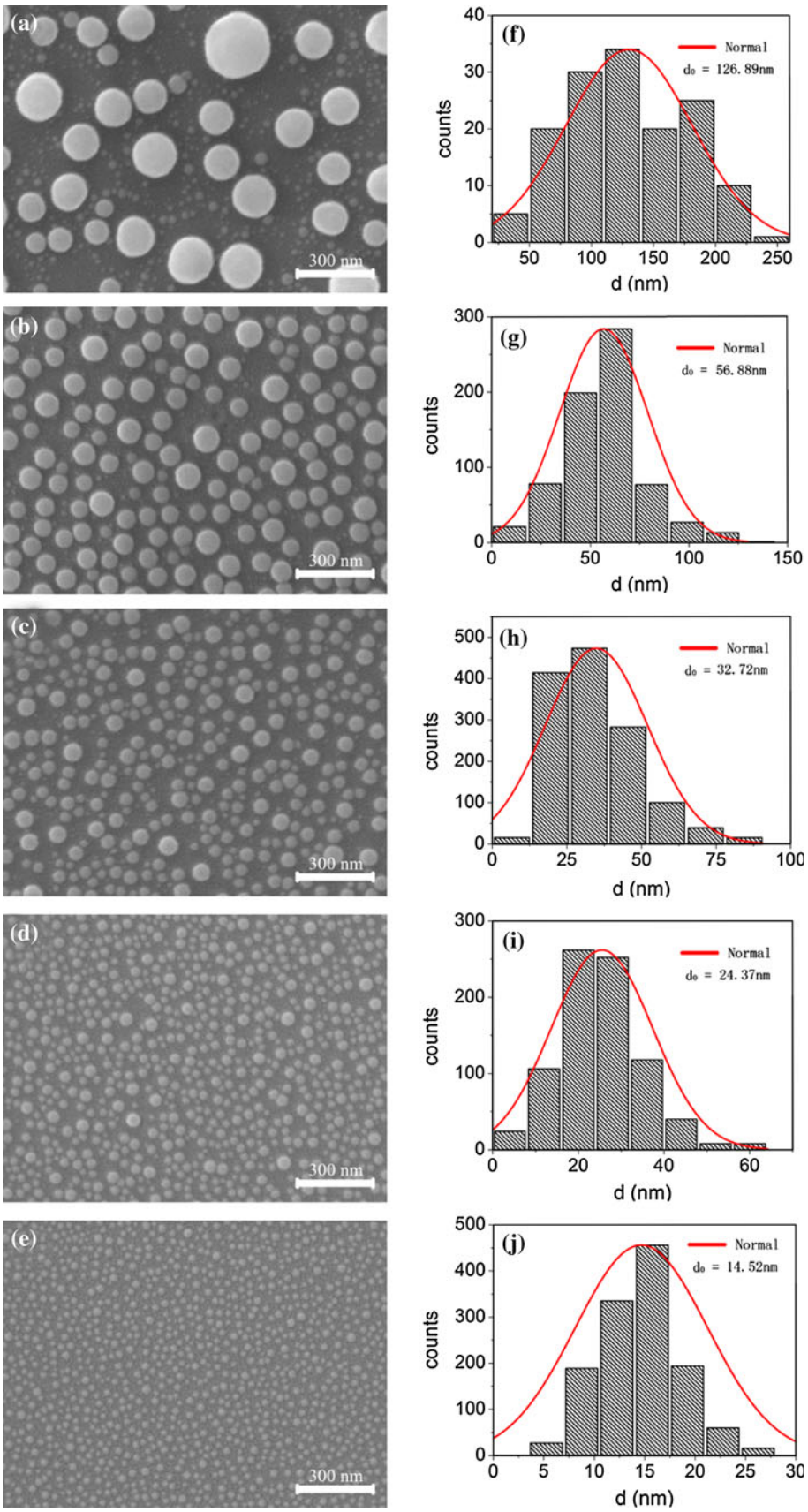

Fig. 1 **a–e** SEM images of the sample #1–5. The images show nearly spherical Ni nanoparticles spread on the Si substrate homogeneously. **f–j** Histograms of the Ni nanoparticle size distributions for sample #1–5 determined by SEM images. *Solid lines* are the fittings based on a normal distribution

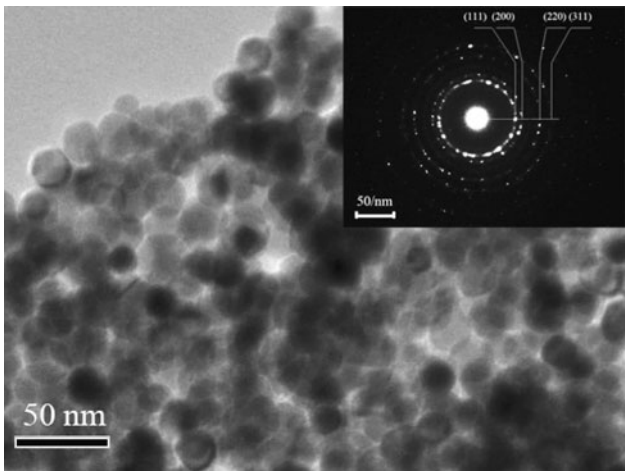

Fig. 2 Bright field TEM micrograph of the particles scraped off sample #4 where the *inset* shows the electron diffractogram of the samples

the thickness of the Ni thin film. Hence, the diameter of Ni nanoparticles can be estimated by

$$d \approx 3t_{\mathrm{Ni}} = 3 \cdot \frac{Z_{\mathrm{Ni}}}{Z_{\mathrm{NiO}}} \cdot \frac{\rho_{\mathrm{NiO}}}{\rho_{\mathrm{Ni}}} \cdot t_{\mathrm{NiO}} = 1.74 t_{\mathrm{NiO}}, \quad (1)$$

where t_{Ni} and t_{NiO} denote the thickness of Ni film and NiO film, Z_{Ni} (58.69) and Z_{NiO} (74.70) are the relative molecular weight of Ni and NiO, ρ_{Ni} (8.9×10^3 kg/m^3) and ρ_{NiO} (6.6×10^3 kg/m^3) are the density of Ni and NiO. In our works, it can be observed that the median particle diameters of sample #1–5 are 126.89, 56.88, 32.72, 24.37, and 14.52 nm (see Fig. 1), respectively. The relationship between particle diameters of the samples and the thicknesses of the original NiO films before annealing is shown in Fig. 4. The sizes of this Ni nanoparticles are all approximate values and little lower than theory values. The possible reason is that, small amount of Ni is volatilized in

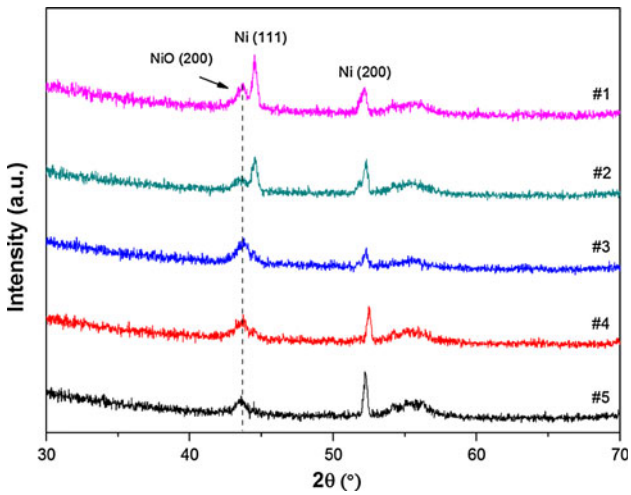

Fig. 3 Grazing incidence X-ray diffraction patterns for sample #1–5

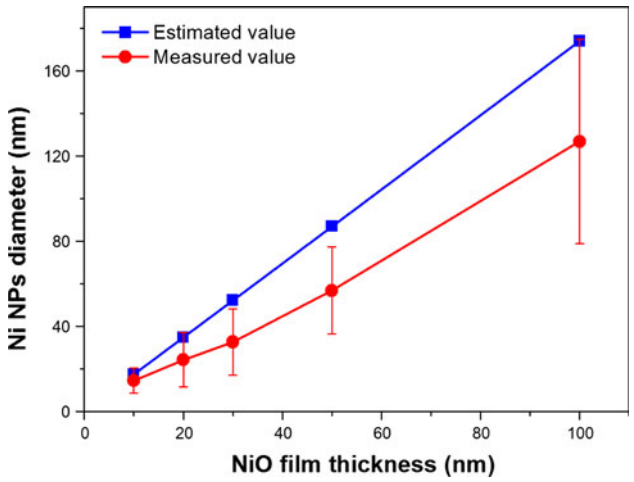

Fig. 4 The relationship between particle diameters of the samples and the thicknesses of the original NiO films before annealing

the process of Ni being reduced at high temperature, which made the actual thickness of Ni film is thinner than the theoretical value. Therefore, the actual sizes of the Ni nanoparticles are smaller than the theory value. But the particle sizes have an approximate linear relationship with the films thickness which is consistent with the theory. So, the Ni nanoparticle size can be well controlled by controlling the sputtering thickness of the NiO film.

The Ni nanoparticles of different sizes in our samples show different magnetic properties. Figure 5 shows the magnetic hysteresis loops of samples #1–5 at 300 K with Ni nanoparticles of different sizes on the substrate. Coercivity H_{C} is defined in terms of two field values H_{left} and H_{right} where magnetic moment $M = 0$: $H_{\mathrm{C}} = (H_{\mathrm{right}} - H_{\mathrm{left}})/2$. It is found that H_{C} falls with the decrease of Ni nanoparticle size, and when the size is smaller than

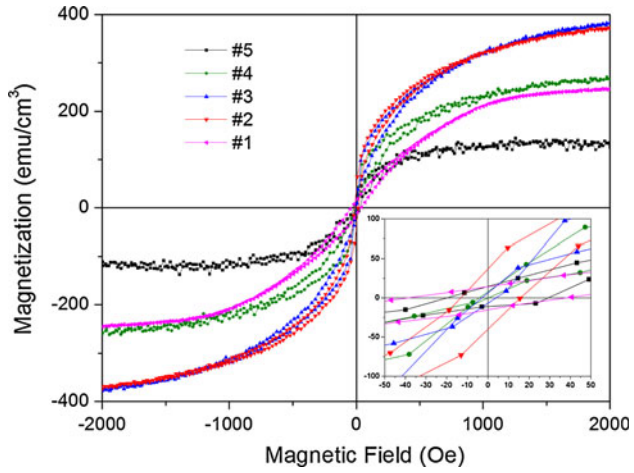

Fig. 5 The magnetic hysteresis loops of sample #1–5 measured with VSM at 300 K, where the *inset* shows the magnification of the loops around the coercive field

30 nm, it becomes difficult to measure H_C with VSM and H_C is considered to be approaching zero. The behavior of the Ni nanoparticles below ac. 30 nm is similar to that of a paramagnetic material. Ni is a prototype of FM material but when it is below its critical radius R_C, thermal agitation will lead to a superparamagnetic state instead of stable magnetization. For each temperature T, there is a critical radius R_C (T), which marks the limit between the superparamagnetic particles ($R < R_C$ (T)) and the blocked ones ($R > R_C$ (T)). Hence, the critical radius R_C at room temperature obtained from our samples is smaller than 15 nm which is close to the theoretical value [24, 25].

The Ni nanoparticles of sample #4 exhibit superparamagnetic properties at room temperature, and the coercivity H_C of sample #4 is further measured in the temperature range of 5–300 K, as shown in Fig. 6a. The coercivity can not be detected once the temperature rises above 100 K. The coercivity increases with the decrease of temperature when temperature drops below 100 K. Particles smaller than R_C have a characteristic temperature called blocking temperature T_B, below which the magnetization is stable with well-defined H_C, while above T_B the magnetization is highly unstable with no H_C. The value of blocking temperature of Ni nanoparticles on sample #4 can be determined as ac. 100 K by the changes in coercivity. The temperature dependence of H_C for randomly oriented noninteracting superparamagnetic particles below T_B is given by the relation [26]

$$H_C = \alpha \frac{2K}{M_S}\left[1 - \left(\frac{T}{\langle T_B \rangle}\right)^{1/2}\right] = \alpha \frac{2K}{M_S} - \frac{10\alpha}{M_S}\left(\frac{k_B K}{\langle V \rangle}\right)^{1/2} T^{1/2}, \quad (2)$$

where M_S (483 emu/cm^3) is the saturation magnetization of Ni, K is the effective anisotropy constant of the particles with the mean volume $\langle V \rangle$, and $\alpha = 1$, if the particle easy axes are aligned or $\alpha = 0.48$, if randomly oriented. The model used to evaluate the blocking temperature and particles size is correct for an ideal system of magnetic monodomains in the blocked state (Stoner and Wohlfarth model [27, 28]) when the following assumptions are made: (i) monodisperse nanoparticles system with uniaxial anisotropy; (ii) random distribution of easy axis; and (iii) coherent reversal of the magnetic moments of the particles. Eq. 2 can estimate the coercivity of the sample roughly. Function

$$H_C(T) = P_1 - P_2 T^{1/2} \quad (3)$$

is used to fit the data of temperature dependence of coercivity H_C. Here P_1 and P_2 are fitting parameters. The fitting line and coercivity H_C of sample #4 below 100 K are shown in Fig. 6b The values of P_1 and P_2 given by fitting are 214.00 Oe and 21.54 Oe/K$^{1/2}$. The calculated value of T_B is 98.75 K according to P_1 and P_2, very close to the estimated value obtained from coercivity measurements, and from P_1 and P_2, the median particle diameter d can be calculated as

$$\langle d \rangle = (6\langle V \rangle/\pi)^{1/3} = (600\alpha^2 k_B K/\pi P_2^2 M_S^2)^{1/3} = 17.94\,\text{nm}, \quad (4)$$

which is also close to the median particle diameter shown in Fig. 1. From Eq. 2 and value P_1, the value of effective anisotropy constant K is 1.08×10^5 erg/cm^3. Fitting coercivity values at different temperatures below the blocking temperature is one experimental method to obtain the effective anisotropy constant of the particles. Thus, the experimental value is significantly larger than that of the bulk Ni [29]. Such large effective anisotropy may be partly due to the "core–shell" particle morphology where the

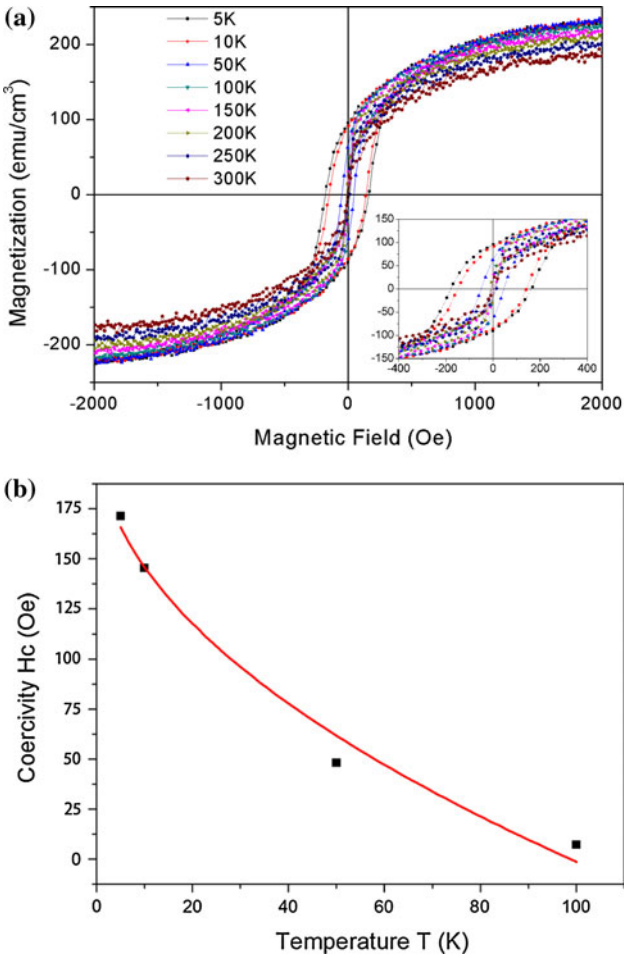

Fig. 6 **a** The magnetic hysteresis loops of sample #4 measured by VSM in the temperature range of 5–300 K, where the *inset* shows the magnification of the loops around the coercive field. **b** The coercivity H_C of sample #4 decreases with increasing temperature T below 100 K. *Solid line* is the fitting based on Eq. 2

oxide coating is believed to interact strongly with the Ni core ("interface effect") and partly due to the marked contribution of the surface anisotropy ("surface effect") which is expected in nanoparticles [11].

Conclusion

Single layer Ni nanoparticles with various sizes were prepared with an easy new method, and the nanoparticle size can be precisely controlled by adjusting the magnetron sputtering time. The hysteresis loops of five sizes of Ni nanoparticles were obtained at room temperature, and when the size is below ac. 30 nm, the coercivity will approach zero. The coercivities of the ca. 20 nm Ni nanoparticles were measured in the temperature range of 5–300 K, within which the nanoparticles show typical superparamagnetic properties. The blocking temperature T_B and particle size were calculated by fitting the relationship between coercivity and temperature, whose values were close to the direct experimental results. The effective anisotropy constant can also be obtained with this method, and its value is significantly larger than that of the bulk Ni. The magnetic properties of these Ni nanoparticles can be significantly influenced by the particle sizes. Moreover, the single layer Ni nanoparticles with controllable size are one good catalyst for carbon nanotubes, and the single layer Ni nanoparticles can be mingled into other films or devices uniformly to modulate their optical, electrical and magnetic properties, enabling the Ni nanoparticles to have more potential applications.

Acknowledgements The author thanks the National Basic Research Program of China (973 Program, No. 2009CB939704), the National Nature Science Foundation of China (Nos. 10905043, 11005082), the Specialized Research Fund for the Doctoral Program of Higher Education (No. 20100141120042), Young Chenguang Project of Wuhan City (Nos. 200850731371, 201050231055), and the Fundamental Research Funds for the Central Universities.

References

1. Gubin SP, Koksharov YA, Khomutov GB, Yurkov GY (2005) Russ Chem Rev 74:489
2. Klabunde KJ (2001) Nanoscale materials in chemistry. Wiley, New York
3. Schmid G (2004) Nanoparticles from theory to application. Willey-VCH, Weinheim
4. Battle X, Labarta A (2002) J Phys D 35:R15
5. Rancourt DG (2001) Rev Miner Geochem 44:217
6. Bedanta S, Kleemann W (2009) J Phys D 42:013001
7. Guéron S, Deshmukh MM, Myers EB, Ralph DC (1999) Phys Rev Lett 83:4148
8. Liou SH, Huang S, Klimek E, Kirby RD, Yao YD (1999) J Appl Phys 85:4334
9. Martinez B, Obradors X, Balcells L, Rouanet A, Monty C (1998) Phys Rev Lett 80:181
10. Nogues J, Skumryev V, Sort J, Stoyanov S, Givord D (2006) Phys Rev Lett 97:157203
11. Gubin SP (2009) Magnetic nanoparticles. Willey-VCH, Weinheim
12. Bi L, Li S, Zhang Y, Youvei D (2004) J Magn Magn Mater 277:363
13. Cıntora-Gonzalez O, Estournes C, Richard Pionet M, Guille JL (2001) Mater Sci Eng C 15:179
14. Wang WN, Yoshifimi I, Wuled-Lengorro I, Okuyama K (2004) Mater Sci Eng B 111:69
15. Doppiu S, Langlais V, Sort J, Surinach S, Baro MD, Zhang Y, Hadjinapayis G, Nogue's J (2004) Chem Mater 16:5664
16. Sharma SK, Vargas JM, Knobel K, Pirota KR, Meneses CT, Kumar S, Lee CG, Pagliuso PG, Rettori C (2010) J Appl Phys 107:09D725
17. Zhou YZ, Chen JS, Tay BK, Hu JF, Chow GM, Liu T, Yang P (2007) Appl Phys Lett 90:043111
18. D'Addato S, Gragnaniello L, Valeri S, Rota A, Bona A, Spizzo F, Panozaqi T, Schifano SF (2010) J Appl Phys 107:104318
19. Yudasaka M, Kikuchi R, Matsui T, Ohki Y, Yoshimura S, Ota E (1995) Appl Phys Lett 67:2477
20. Sanjabi S, Faramarzi A, Hamdam Momen M, Barber ZH (2009) J Phys Chem C 113:8652
21. Jiang Q, Wang YW, Li JC (1999) Appl Surf Sci 152:156
22. Liang LH, Liu F, Shi DX, Liu WM, Xie XC, Gao H (2005) Phys Rev B 72:035453
23. Sanjabi S, Faramarzi A, Hamdam Momen M, Barber ZH (2008) J Phys Chem Solids 69:1940
24. Kittel C (1949) Rev Mod Phys 21:541
25. Kitell C, Galt JK, Campbell WE (1950) Phys Rev 77:725
26. Kneller EF, Luborsky FE (1963) J Appl Phys 34:656
27. Stoner EC, Wohlfarth EP (1948) Philos Trans R Soc A 240:599
28. Nunes WC, Folly WSD, Sinnecker JP, Novak MA (2004) Phys Rev B 70:014419
29. Aharoni A (2001) J Appl Phys 90:4645